Int. J. Electrochem. Sci., 13 **(2018)** 7095 – 7110, doi: 10.20964/2018.07.74

International Journal of
ELECTROCHEMICAL
SCIENCE
www.electrochemsci.org

Effects of Sensitization on the Metastable Pitting Corrosion of 304 Stainless Steel

Yan Hou, Congqian Cheng[*]*, Tieshan Cao, Xiaohua Min, Jie Zhao*

School of Materials Science and Engineering, Dalian University of Technology, Dalian 116024, China
[*]E-mail: cqcheng@dlut.edu.cn

Received: 9 April 2018 / *Accepted:* 23 May 2018 / *Published:* 5 June 2018

The effects of sensitization on the metastable pitting behaviour of 304 stainless steel in 3.5 wt.% NaCl solution were investigated via electrochemical measurements and microscopic observations. Results showed that sensitization decreased pitting potential and slightly affected metastable pitting potential. Sensitization treatment increased the nucleation frequency of metastable pitting, promoted its propagation and changed the shape of current transients. The results of scanning electron microscopy and energy-dispersive X-ray spectroscopy showed that metastable pitting was initiated at MnS inclusions for the solution-treated and sensitized samples. The combined effects of the passive film and inclusions were considered to play a vital role on the metastable pitting behaviour.

Keywords: stainless steel, sensitization, passive film, metastable pitting, inclusion

1. INTRODUCTION

Austenitic stainless steel is widely used in harsh environments due to its high corrosion resistance [1, 2]. However, this type of steel suffers from pitting corrosion under the attack of aggressive chloride ions. In general, pitting corrosion is characterised by three steps: pitting initiation, metastable pitting and stable pitting [3]. Metastable pitting, as the precursor state to stable pitting, has been investigated extensively.

Metastable pitting behaviour is closely related to potential [4], environmental conditions [5-8] and alloy microstructure [9, 10]. Tian et al. [4] reported that the lifetime, peak current and nucleation number of metastable pitting increased with the applied potential in stainless steel. Moayed et al. [5] found that a high temperature would accelerate pit growth near the critical pitting temperature. Naghizadeh et al. [6] showed that dichromate ions decreased the initiation and growth of a metastable pit. Guan et al. [7] investigated the effect of cyclic stress on the metastable pitting behaviour of 304

stainless steel. Bai et al. [9] reported that the addition of Boron accelerated the formation of metastable pits and increased the probability of stable pitting. Liu et al. [10] determined that nanocrystallization increased the frequency of metastable pit formation and decreased the rate of stable pitting nucleation and growth.

Active sites in stainless steel, such as inclusions or any place with a diminished passive film, play important roles in pitting corrosion [11-13]. MnS inclusions and Cr-depleted zones are two typical active sites for metastable pitting initiation. MnS inclusions can be dissolved under the catalyzation of chloride ions, and thus prefer the formation of metastable pits [14]. Sensitization is a phenomenon in which Cr-depleted zones occur at the region adjacent to the grain boundaries [2, 15]. Although many studies have reported the increase in pitting susceptibility as a result of sensitization treatment [2, 16, 17], metastable pitting behaviour has not been systematically elucidated. Pitting attack always occurs at the grain boundaries and the precipitate/matrix interfaces because of the precipitation of $Cr_{23}C_6$ carbides [18]. The formation and propagation of pits along sensitized grain boundaries were also verified under the droplet condition of 304 stainless steel in our previous work [19]. Ida et al. [20] recently reported that pits were still initiated at MnS inclusion via microscopy observation, although sensitization decreased pitting resistance. Therefore, elucidating metastable pitting behaviour under the effect of sensitization is a significant and interesting endeavour.

In the present study, the metastable pitting behaviour of 304 stainless steel under various degrees of sensitisation (DOS) was investigated via potentiodynamic polarisation, electrochemical impedance spectroscopy (EIS) and potentiostatic polarization. The current transient profile and statistical probability of metastable pits were analysed to understand their initiation and propagation processes. The morphology and electrochemical behaviour of metastable pits were also discussed.

2. EXPERIMENTAL PROCEDURES

2.1 Preparation of samples

Specimens with dimensions of 15 mm × 10 mm were cut from a 3 mm-thick commercial 304 stainless steel plate. The chemical composition in weight percentage (wt.%) was 0.05 C, 0.54 Si, 1.09 Mn, 7.74 Ni, 18.05 Cr, 0.03 Mo, 0.041 P, 0.005 S and a balance of Fe. All the specimens were solution-treated at 1100 °C for 1 h and then water quenched. Sensitization heat treatment was conducted on all the specimens at 670 °C for 1, 4 and 24 h, and then the specimens were quenched in water. The samples were cold-mounted in epoxy resin, and electrical contacts were connected with a Cu wire at the back of the samples. For each electrochemical experiment, the specimen surface was abraded with SiC emery papers (180 grit to 1500 grit) and then polished with 1.5 μm diamond paste. Afterwards, the specimens were washed with ethanol and deionised water, and finally dried under warm air.

The samples were electrochemically etched in 10 wt.% oxalic acid at a current density of 1 A/cm^2 for 90 s according to ASTM standard A-262 Practice A. The microstructure of the solution-treated and sensitized samples was examined via optical microscopy.

2.2 Electrochemical procedures

All electrochemical polarization experiments were performed using a CS350 electrochemical workstation at 20 ± 2 °C. Tests were conducted in a naturally aerated 3.5 wt.% NaCl solution using a three-electrode electrochemical cell, where Ag/AgCl (SSE) and a platinum sheet were used as the reference and counter electrodes, respectively. The open circuit potential (OCP) was obtained for 15 min before each polarization test.

DOS was evaluated via the double-loop electrochemical potentiokinetic reactivation (DL-EPR) technique in 0.5 M H_2SO_4 and 0.01 M KSCN solution, and the scanning rate was 100 mV/min. The samples were polarized from OCP to 0.3 V_{SSE}, and then scanning direction was reversed until OCP. DOS was evaluated using the ratio of current density (i_r/i_a) [21], where i_r is the maximum reactivation current density and i_a is the maximum activation current density. The DL-EPR test was repeated thrice for each specimen.

Potentiodynamic measurements were conducted by sweeping the potential from 30 mV below OCP at a scan rate of 0.2 mV/s until the current density exceeded 0.1 mA/cm^2. The data acquisition rate was 10 Hz, and no data smoothing was applied. The samples were immersed in the solution for 2 h to form a stable passive film before EIS measurements. EIS measurements were conducted at a frequency ranging from 10^5 Hz to 10^{-2} Hz with an AC signal amplitude of 10 mV.

Current transients were measured through potentiostatic tests with an applied potential of 0.3 V_{SSE}. To avoid crevice corrosion, silica gel was applied along the specimen/epoxy resin interface. The final exposed area of the sample was 0.2 cm^2. Current transients were recorded for 3600 s at a frequency of 50 Hz. Polarization tests were repeated six times under each identical sensitization conditions to ensure their reproducibility. In addition, scanning electron microscopy (SEM) with energy-dispersive X-ray spectroscopy (EDX) was adopted to observe the morphology and initiation sites of metastable pits.

3. RESULTS

3.1 Microstructure and DOS after sensitization treatment

Fig. 1 shows the optical microscope images of 304 stainless steel after sensitization treatment at 670 °C. The slight step structure was observed between the austenitic grains of the solution-treated specimen, as shown in Fig. 1(a). After sensitization for 1 h, the dual structure, some ditches at grain boundaries in addition to steps were presented, but no single grain was completely surrounded by ditches, as shown in Fig. 1(b). Additionally, when the sensitization period was prolonged, it revealed the ditch structure presented by deep intergranular attack, as shown in Figs. 1(c) and 1(d). This fact was due to chromium carbide developed at intergranular and caused Cr-depleted zones adjacent the grain boundaries after sensitization treatment, and therefore, with increasing of sensitization time, suggesting a large extent of intergranular corrosion [2].

Fig. 2 shows the DOS of 304 stainless steel obtained from the DL-EPR tests. Significant reactivation peaks in the polarization loops during reverse scanning were verified for the sensitized samples. Such high peaks indicated high DOS after sensitization treatment. However, no evident peak was observed for the solution-treated sample, as shown in Fig. 2(a). Based on the DL-EPR curves, the calculated DOS values increased with sensitization time. It seems that nearly no sensitization susceptibility for the solution-treated samples as shown in Fig. 2(b).

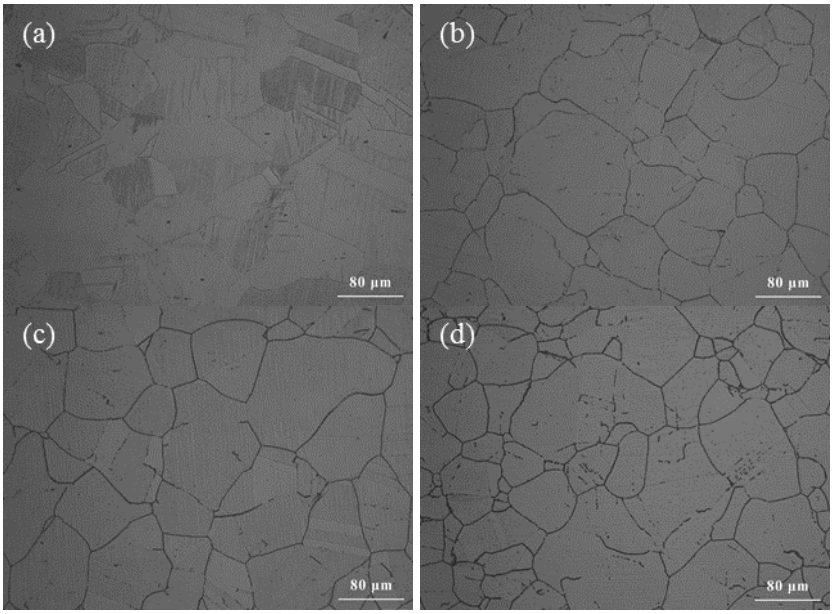

Figure 1. Optical microscope images of the solution-treated and sensitized 304 stainless steel after electrochemical etching in 10% oxalic acid: (a) solution-treated, (b) sensitized for 1 h, (c) sensitized for 4 h and (d) sensitized for 24 h.

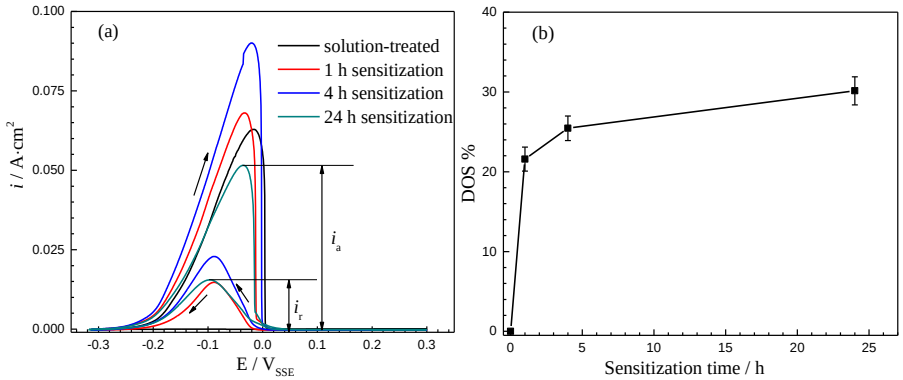

Figure 2. (a) DL-EPR curves and (b) DOS values of the solution-treated and different sensitized samples of 304 stainless steel at 670 °C.

3.2 Potentiodynamic polarization and EIS measurements

Fig. 3(a) depicts the typical potentiodynamic polarization curves of 304 stainless steel in 3.5 wt.% NaCl solution. Current fluctuations in the passive region were regarded as metastable pitting,

whilst current density increased dramatically, thereby indicating the occurrence of stable pitting [22, 23]. Sensitization treatment slightly increased passive current density and apparently enhanced metastable pitting reactivity in the passive region. As shown in the enlargement of point B (image inserted in Fig. 3(a)), a deviation of 0.06 μA/cm^2 from the background of passive current was selected as the standard of a metastable nucleation event. The potential at the first event during anodic polarization was defined as the metastable pitting potential (E_m). As shown in Fig. 3(b), the stable pitting potential (E_p) sharply declined from 0.53 V to 0.41 V with an increment in sensitization time and lineally decreased with an increase in DOS values. However, no evident change in E_m was detected via the sensitization treatment.

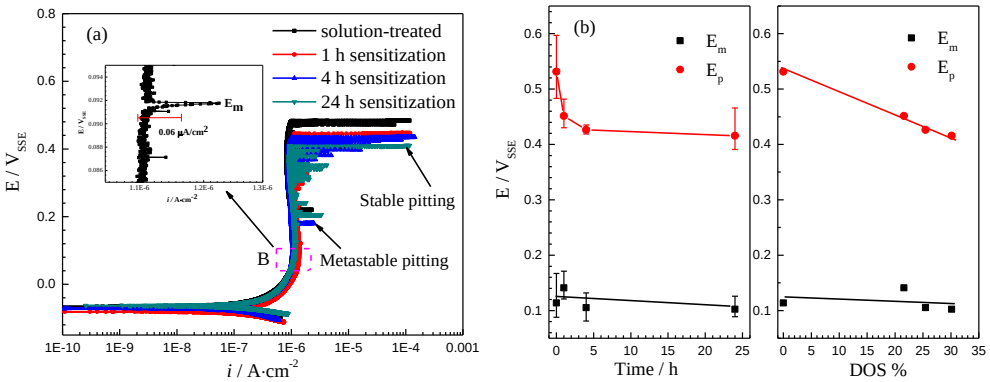

Figure 3. (a) Potentiodynamic polarization curves of 304 stainless steel in 3.5 wt.% NaCl solution and (b) change in metastable and stable pitting potentials with sensitization treatment.

Fig. 4 shows the Nyquist plots from the EIS measurements. The Nyquist plots exhibited a depressed semicircle, characterized as semicircle capacitive loops, in nearly all the measured frequency regions, thereby indicating a similar corrosion mechanism. The diameter of the capacitive loops decreased with sensitization time, which indicated a decrease in the stability of the passive film caused by the sensitization treatment [24, 25].

$$Z(w) = Z_0 \cdot (jw)^{-n}$$

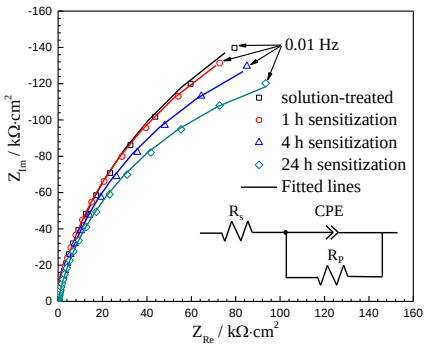

Figure 4. Nyquist plots and equivalent circuit model of the solution-treated and sensitized specimens in 3.5 wt.% NaCl solution.

The proposed equivalent circuit model for fitting EIS data is presented in Fig. 4 to quantify the electrochemical parameters. In this model, R_s represents electrolyte resistance, CPE denotes double charge layer capacitance and R_P indicates the resistance of the passive film. CPE was used in this model due to the non-ideal nature of the interface [26]. The impedance of CPE can be generally defined as

$$Z(w) = Z_0 \cdot (jw)^{-n}, \quad (1)$$

where Z_0 is the admittance magnitude of CPE, ω is the angular frequency and n is the CPE exponent. The fitted EIS parameters obtained from Fig. 4 are presented in Table 1. The passive film resistance (R_p) decreased with an increase in sensitization time at 670 °C.

Table 1. Fitted parameters obtained from the EIS plots of 304 stainless steel

Material	R_s / Ω·cm^2	CPE / Ω^{-1}·cm^{-2}·s^n	n	R_p / Ω·cm^2
solution-treated	6.81	2.72×10^{-5}	0.910	4.39×10^{5}
1 h sensitization	6.89	3.36×10^{-5}	0.921	4.01×10^{5}
4 h sensitization	6.56	2.71×10^{-5}	0.911	3.51×10^{5}
24 h sensitization	6.56	2.22×10^{-5}	0.902	3.03×10^{5}

3.3 Potentiostatic polarization characteristics

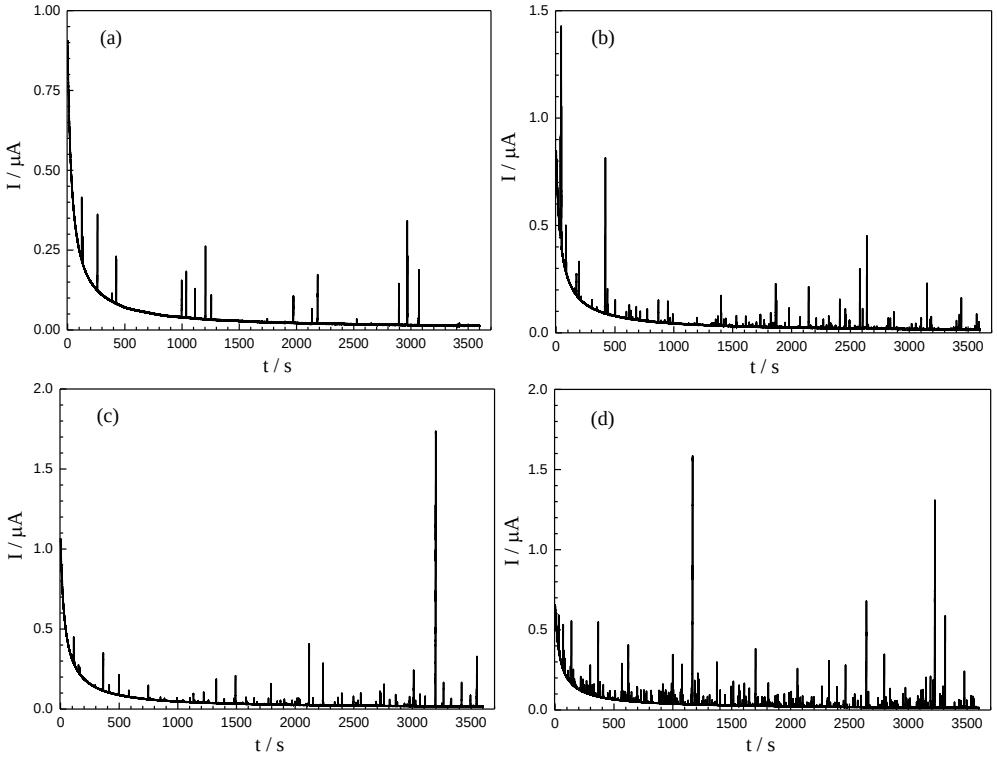

Figure 5. Current transients of 304 stainless steel in 3.5 wt.% NaCl at an applied anodic potential of 0.3 V_{SSE}: (a) solution-treated, (b) sensitized for 1 h, (c) sensitized for 4 h and (d) sensitized for 24 h.

Fig. 5 illustrates the current transient versus time records of the solution-treated and sensitized 304 stainless steel specimens collected at 0.3 V_{SSE}. For all the samples, the background current sharply decayed during the first 500 s and then gradually decreased with time. The number of metastable pitting peaks presented by the current transients increased because of sensitization. In particular, the maximum amplitude in the transient peaks was enhanced by sensitization. This result indicates that sensitization may significantly affect the growth of metastable pitting.

Most metastable events belong to three categories according to their behaviour, i.e. the growth kinetic exponent n, where n can be fitted from the dissolution current I(t) and time t follows a power law: $I(t) \sim t^n$ [5]. Fig. 6 shows the typical shape of the individual current transient observed for the solution-treated and 24 h sensitized samples that are selected from Figs. 5(a) and 5(d). The log–log relationship between I(t) and t for the individual current transient is inserted into Figs. 6(a), 6(b) and 6(c). In addition, Fig. 6(a) illustrates the current transients of the metastable pits developed on 304 stainless steel and graphically describes the key characteristics of the transient: pit peak current (I_{peak}), pit growth time, pit repassivation time and metastable pit lifetime.

In Type A profile, the current increases abruptly until it reaches a plateau of constant current, then a sharp increase followed by a sudden repassivation occurs, as shown in Fig. 6(a). The calculated n values vary from 1.7 to 0.36 and then change to 2.14. Fig. 6(b) depicts Type B current transient

characterized by a continuous and stepwise increase in the current, followed by an abrupt repassivation. The calculated n values are below 1. The lifetime of the current transients of Types A and B is long and may be attained by approximately 6 s. Compared with Types A and B transient peaks, the feature of Type C transient is characterized by a narrow peak with a lifetime that is considerably shorter than 1 s and an n value above 1.

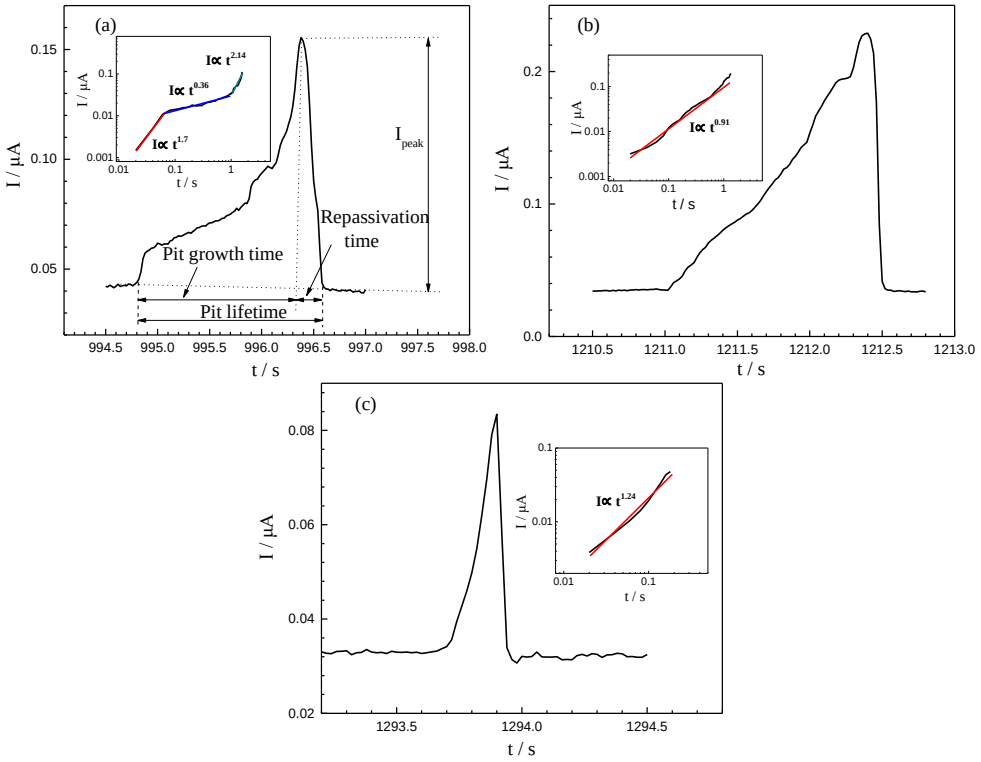

Figure 6. Analysis of individual current transients observed for the solution-treated and 24 h sensitized samples at 0.3 V_{SSE}. (a) Type A, (b) Type B and (c) Type C. The inset figure shows the log–log relationship between I(t) and t for the current transient.

Fig. 7 illustrates the probability of appearance of the three transient types for the samples subjected to solution treatment and 24 h sensitization treatment. The occurrence probability of type C transients was increased from 5% to 30% after 24 h of sensitization treatment. This result indicates that sensitization may change growth behaviour due to high occurrence probability of metastable events with n above 1.

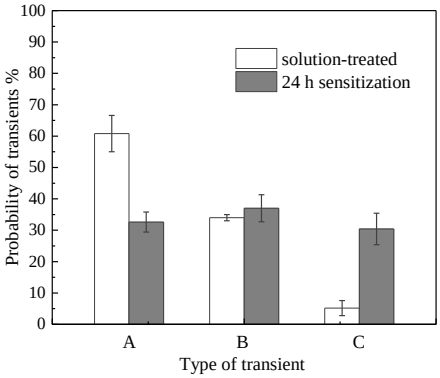

Figure 7. Probability of appearance of different types of current transients for the solution-treated and 24 h sensitized samples at 0.3 V_{SSE}.

3.4 Statistical analysis of metastable events

Fig. 8 represents the average frequency of pit initiation λ ($cm^{-2}·s^{-1}$) for the solution-treated and sensitized samples at 0.3 V_{SSE}, where the number of current transients was counted over 200 s intervals. The large error bars indicated that metastable pitting was a highly random process. In general, sensitization treatment increased metastable pit initiation frequency. In particular, nearly high values of λ could be achieved within 3600 s for the 24 h sensitized samples, as shown in Fig. 8.

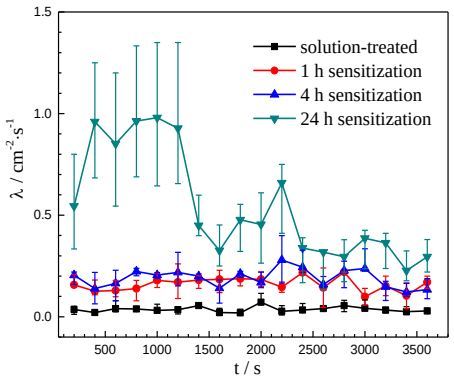

Figure 8. Metastable pit frequency λ with prolonged sensitization time during the potentiostatic polarization of 304 stainless steel at 0.3 V_{SSE} in 3.5 wt.% NaCl solution.

Fig. 9 shows the cumulative probability plot of the I_{peak} for the solution-treated and sensitized specimens at 0.3 V_{SSE} in 3.5 wt.% NaCl solution. The cumulative probability of the I_{peak} was calculated by using a mean rank method as n/(N + 1), where N is the total number of pits and n is the order in the total number [27]. The median value of I_{peak} for the solution-treated samples was 2.8 times higher than that for the sensitized samples. Some of the metastable pits for the sensitized samples exhibited I_{peak} values higher than 0.3 μA (some even reached 1.6 μA) after sensitization treatment, but the I_{peak} values for the solution-treated samples was within the range of 0.3 μA. These results indicated that sensitization treatment extended I_{peak} towards a higher value range for metastable pit growth.

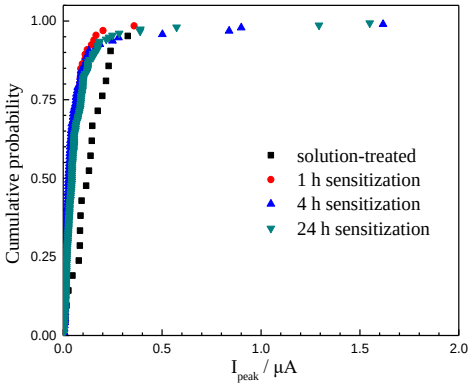

Figure 9. Cumulative probability of metastable pit peak current for the solution-treated and sensitized samples obtained from potentiostatic polarization at 0.3 V_{SSE} in 3.5 wt.% NaCl solution.

The lifetime of a metastable pit is regarded as the time when metastable current transients begin to increase until they decrease to the background current. Fig. 10 shows the cumulative probability distribution of metastable pit lifetime for the solution-treated and sensitized specimens at 0.3 V_{SSE} in 3.5 wt.% NaCl solution. The 24 h sensitized specimens exhibited longer metastable pit lifetime (approximately 6 s), thereby indicating that sensitization treatment promoted the propagation of metastable pits. However, the median value of metastable pit lifetime was significantly decreased by sensitization treatment. The shorter lifetime of metastable pits for the sensitized specimen implied that further growth of these pits ceased and repassivation was relatively robust.

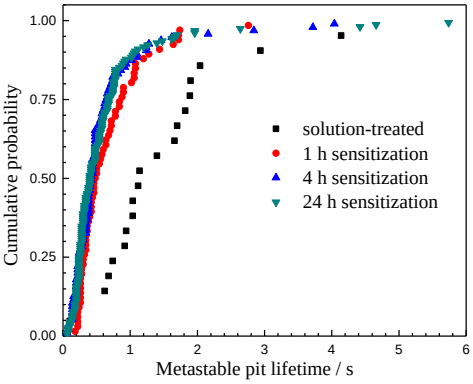

Figure 10. Cumulative probability of metastable pit lifetime for the solution-treated and sensitized samples obtained from potentiostatic polarization at 0.3 V_{SSE} in 3.5 wt.% NaCl solution.

Assume that the pit is hemispherical. The metastable pit radius r_{pit} can be calculated using Faraday's equation, as follows (2) [7]:

$$r = \left(\frac{3QM}{2\pi nF\rho}\right)^{\frac{1}{3}}, \qquad (2)$$

where Q is the integral charge from the background current to the peak current, and F is the Faraday constant of 96,485 C/mol. For 304 stainless steel, the mean valence state n of metal cations

was assumed to be 2.19, the density ρ was 7.93 g/cm^3 and the molar mass of the alloy M was 55.83 g/mole, as reported in the literature [4]. Fig. 11 shows the cumulative probability distribution of pit radius for the solution-treated and sensitized samples at 0.3 V_{SSE} in 3.5 wt.% NaCl solution. Notably, metastable pits with a radius larger than 2 μm existed in the sensitized specimens, which were considerably larger than that in the solution-treated specimens. However, the median value of r_{pit} was decreased after sensitization treatment. This result showed that sensitization promoted the growth of metastable pits.

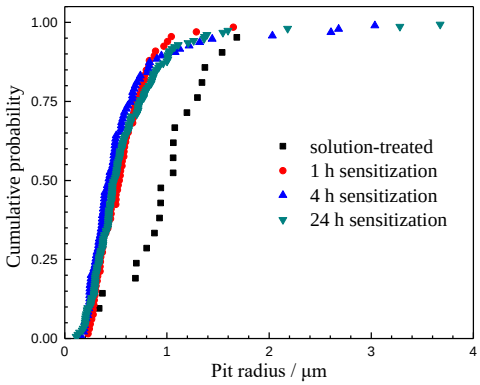

Figure 11. Cumulative probability of metastable pit radius for the solution-treated and sensitized samples obtained from potentiostatic polarization at 0.3 V_{SSE} in 3.5 wt.% NaCl solution.

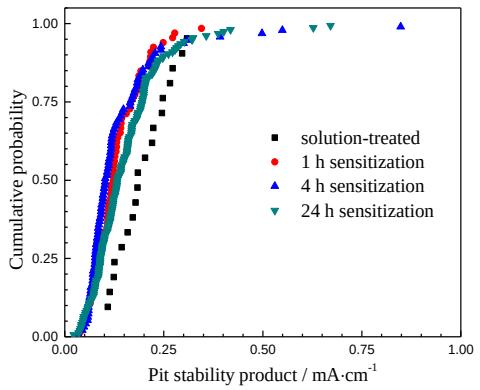

Figure 12. Cumulative probability of metastable pit product stability for the solution-treated and sensitized samples obtained from potentiostatic polarization at 0.3 V_{SSE} in 3.5 wt.% NaCl solution.

Product i_{peak}·r must exceed a certain critical value for the pit to grow stably. Product stability can be calculated using Equation (3) [28]:

$$i_{peak} \cdot r = \frac{I_{peak}}{2\pi r^2} \times r, \quad (3)$$

where I_{peak} is a metastable pit peak current (A), and r (m) is the radius of the pit. Fig. 12 shows the cumulative probability of product stability for the solution-treated and sensitized samples at 0.3 V_{SSE}. As indicated in Fig. 12, although the median value of the solution-treated samples had higher

product stability than the sensitized samples, the pit product stability for the sensitized samples shifted to higher values compared with that for the solution-treated samples, and the highest pit product stability for the sensitized samples was nearly 0.85 mA/cm. Pistorius et al. [29] determined the criterion for developing a metastable pit into a stable pit as 3 mA/cm for 304 stainless steel in NaCl solution. This result suggested that sensitization treatment promoted metastable pitting propagation.

3.5 Morphology of metastable pits

Fig. 13 shows the typical SEM morphology of metastable pits in 304 stainless steel after potentiostatic polarization at an applied potential of 0.3 V_{SSE}. The EDX composition analysis of Sites A and B is presented in Table 2. For the solution-treated and sensitized samples, the metastable pits initiated at the non-metallic inclusions containing MnS and oxide inclusions. Fig. 14 depicts the EDX element mapping of the pits presented in Fig. 13(c). The results indicated that for the 24 h sensitized samples, large pits were located at the oxide inclusion sites, and many small pits were arranged in a chain-like distribution [Figs. 13(c) and 13(d)]. The results of the EDX element mapping of these small pits coincided with the matrix, and intergranular corrosion was not detected in this work.

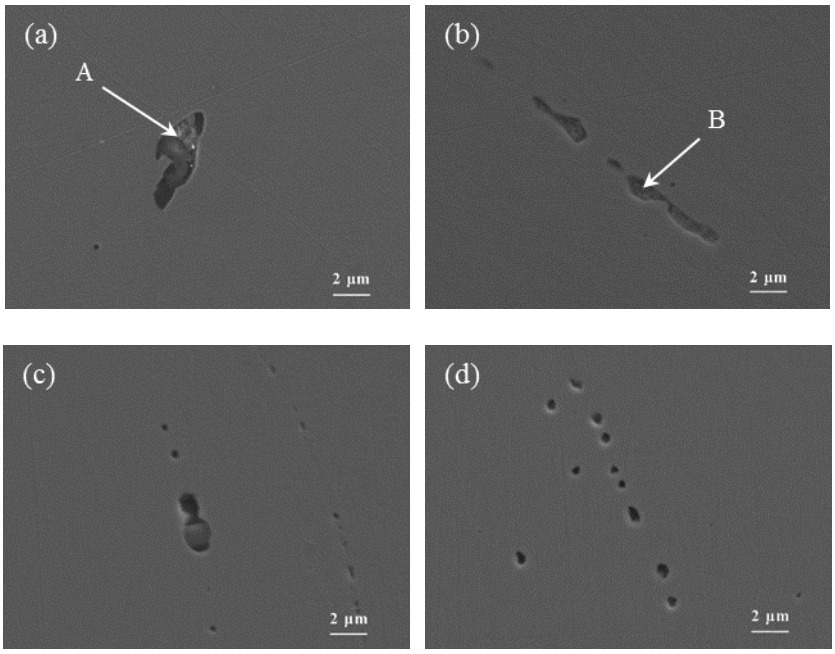

Figure 13. Typical SEM morphologies of metastable pits after conducting potentiostatic tests at an applied potential of +0.3 V_{SSE} in 3.5 wt.% NaCl solution for the (a) solution-treated and (b, c, d) 24 h sensitized specimens.

Table 2. EDX analysis results of Sites A and B in Fig. 13 (wt.%)

Element	O	Al	Si	Ca	S	Mn	Cr	Ni	Fe

A	6.17	1.8	2.19	6.16	14.3	26.4	8.65	2.91	31.42
B	8.14	1.5	2.6	8.86	25.23	33.69	3.2	2.21	14.57

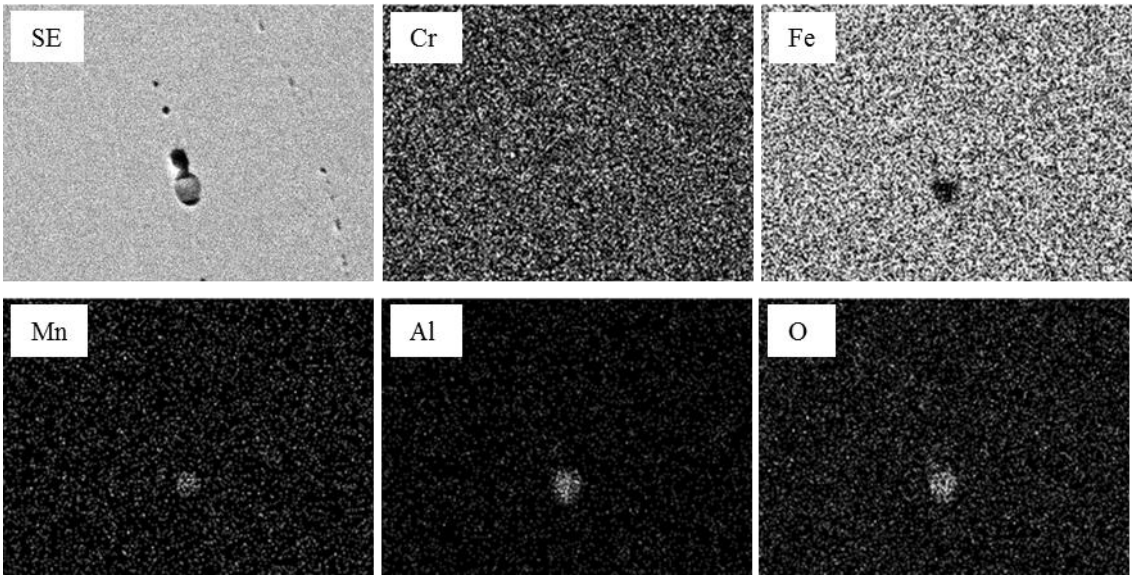

Figure 14. SEM images and element distribution via EDX mapping analysis of Fig. 13(c).

4. DISCUSSION

4.1 Effect of sensitization on metastable pit initiation and propagation

The aforementioned results showed that the initiation frequency of metastable pits increased with sensitization time. The high frequency of metastable pit formation can be related to the inclusions and the stability of the passive film [10, 30]. It was revealed that pits only occured at MnS and mixed MnS/oxide inclusions for 304 stainless steel [31]. However, in the present work, multielement oxide inclusions were also found to initiate pits for the sensitized samples. Thus, many more nucleation points were activated at the inclusion sites after sensitized treatment. Additionally, it is well known that chromium element has a significant role on the protective property of the passive film [32, 33]. The radius of the Nyquist plot decreased for the sensitized samples indicated a decrease in the passive film stability due to the precipitation of intergranular chromium carbide and the occurrence of Cr-depleted zones [2]. The reduction of the chromium content along sensitized grain boundaries decreased the stability of passive film and hence increased the chemical reactivity of those potential sites for pit initiation. Therefore, the increase in the sensitization time would favour more Cr-depleted zones. As a result, the frequency of metastable pitting initiation increased with sensitization time.

Metastable pits initiated at the inclusion sites and intergranular corrosion were not observed in the present work, which suggested that the Cr-depleted zones were not the only reason for pit initiation

at the sensitized grain boundaries, which is in good agreement with the results of Ida et al. [20]. This phenomenon could explain why the values of E_m exhibited no noticeable change with sensitization treatment.

For the solution-treated samples, most of the current transients belonged to Types A and B, which were mainly found on MnS-containing alloys that corresponded to the individual transient initiated at MnS inclusions [34]. For the sensitized samples, however, the calculated r_{pit} of Type C coincided with small pits arranged in a chain-like distribution, which resulted in lower median values of I_{peak}, lifetime and r_{pit} for the sensitized samples than those for the solution-treated samples. The Type C transient of metastable events were likely related to the sensitized grain boundaries. Nevertheless, metastable pits that developed at the sensitized samples with higher I_{peak}, longer lifetime and larger radius belonged to Types A and B. Asano et al. [35] reported that the repassivation ability of Fe-18Cr is relatively high compared to those of Fe-5Cr and Fe-12Cr. Cr content exerted a dominant role on pitting propagation behaviour at MnS inclusions in Fe-Cr steels. Cheng et al. also revealed that sensitization treatment promoted anodic dissolution around the pit sites in 304 stainless steel [19]. Thus, the co-existence of MnS inclusions and Cr-depleted zones at the sensitized grain boundary was likely the major reason for the higher values of the maximum metastable pitting parameters.

4.2 Effect of sensitization on metastable Pitting Stabilization

The sensitized samples had a higher product stability $i_{peak} \cdot r$ than the solution-treated samples. Consequently, the stabilization of metastable pitting was easier after sensitization treatment. Williams et al. [3] proposed that the probability of stable pit formation is directly related to the initiation frequency of metastable events and the probability of repassivation. The relationship between stable pit and metastable pit initiation rates can be expressed as

$$\Lambda = \lambda \exp(-\mu \tau_c), \quad (4)$$

where Λ is the formation rate of a stable pit, λ is the formation rate of metastable pitting, μ is the repassivation probability from metastable pitting and τ_c is the critical time from the metastable pit to the stable pit. Samples with a high initiation frequency of metastable pitting exhibited high probability transition from metastability to stability. Therefore, the effect of sensitization treatment on increasing the frequency of metastable pit initiation directly increased the probability of stable pit formation and decreased the E_p of 304 stainless steel. It can be concluded that increasing sensitization time would lead to decrease the corrosion resistance of the 304 stainless steel.

5. CONCLUSIONS

The effect of sensitization on the metastable pitting behaviour of 304 stainless steel at 670 °C in 3.5 wt.% NaCl solution was investigated via potentiodynamic measurements, EIS, potentiostatic polarization tests and SEM. The results can be summarised as follows.

(1) Potentiodynamic measurements indicated that increasing sensitization time decreased pitting potential and slightly affected metastable pitting potential. The EIS results implied that sensitization treatment decreased the resistance of the passive film.

(2) Potentiostatic measurement indicated that sensitization treatment increased the initiation frequency of metastable pitting. The transients of Type C characterised by a narrow peak and short lifetime significantly increased after sensitization treatment, which resulted in lower median values of I_{peak}, lifetime, r_{pit} and product stability than those for the solution-treated samples. However, sensitization treatment increased the maximum value of the metastable pitting parameter and promoted the propagation of metastable pitting.

(3) The preferential initiation sites were located at the inclusion sites in the solution-treated and sensitized samples. Moreover, many small pits arranged in a chain-like distribution for the sensitized samples were likely to be related to the senzitised grain boundaries.

ACKNOWLEDGEMENTS
This work was supported by National Natural Science Foundation of China (NSFC No. 515701051).

References

1. A. Pardo, M.C. Merino, A.E. Coy, F. Viejo, R. Arrabal and E. Matykina, *Corros. Sci.*, 50 (2008) 1796.
2. M.W.A. Rashid, M. Gakim, Z.M. Rosli and M.A. Azam, *Int. J. Electrochem. Sci.*, 7 (2012) 9465.
3. J. Soltis, *Corros. Sci.*, 90 (2015) 5.
4. W. Tian, N. Du, S. Li, S. Chen and Q. Wu, *Corros. Sci.*, 85 (2014) 372.
5. M.H. Moayed and R.C. Newman, *Corros. Sci.*, 48 (2006) 1004.
6. M. Naghizadeh, D. Nakhaie, M. Zakeri and M.H. Moayed, *Corros. Sci.*, 94 (2015) 420.
7. L. Guan, B. Zhang, X.P. Yong, J.Q. Wang, E.H. Han and W. Ke, *Corros. Sci.*, 93 (2015) 80.
8. H.S. Klapper, J. Goellner, A. Burkert and A. Heyn, *Corros. Sci.*, 75 (2013) 239.
9. G. Bai, S. Lu, D. Li and Y. Li, *J. Electrochem. Soc.*, 162 (2015) C473.
10. L. Liu, Y. Li and F. Wang, *Electrochim. Acta*, 55 (2010) 2430.
11. R. Ke, *J. Electrochem. Soc.*, 142 (1995) 4056.
12. B. Zhang, J. Wang, B. Wu, Y.T. Zhou and X.L. Ma, *Corros. Sci.*, 100 (2015) 295.
13. M.A. Baker and J.E. Castle, *Corros. Sci.*, 23 (1992) 1295.
14. J.R. Kearns, J.R. Scully, P.R. Roberge, D.L. Reichert, and J.L. Dawson, *Electrochemical noise measurement for corrosion applications*, ASTM, (1996) PA, USA.
15. C.S. Kim, S.J. Moon and W.S. Kong, *Mater. Sci. Forum*, 857 (2016) 232.
16. I. Taji, M.H. Moayed and M. Mirjalili, *Corros. Sci.*, 92 (2015) 301.
17. A. Poonguzhali, M.G. Pujar and U. Kamachi Mudali, *J. Mater. Eng. Perform.*, 22 (2013) 1170.
18. Z. Jiang, H. Feng, H. Li, H. Zhu, S. Zhang, B. Zhang, Y. Han, T. Zhang and D. Xu, *Materials*, 10 (2017) 861.
19. C.Q. Cheng, L.I. Klinkenberg, Y. Ise, J. Zhao, E. Tada and A. Nishikata, *Corros. Sci.*, 118 (2017) 217.
20. N. Ida, I. Muto, S. Yu and N. Hara, *J. Electrochem. Soc.*, 164 (2017) C779.
21. N. Ebrahimi, M. Momeni, M.H. Moayed and A. Davoodi, *Corros. Sci.*, 53 (2011) 637.
22. L.F. Garfias-Mesias and J.M. Sykes, *Corros. Sci.*, 41 (1999) 959.
23. Y. Tang, Y. Zuo, J. Wang, X. Zhao, B. Niu and B. Lin, *Corros. Sci.*, 80 (2014) 111.

24. L. Kong, K.S. Wang, Y.P. Zhan and Y. Zhang, *Int. J. Electrochem. Sci.*, (2017) 2973.
25. S. Ningshen and U.K. Mudali, *Electrochim. Acta*, 54 (2009) 6374.
26. I. Frateur, A. Carnot, S. Zanna and P. Marcus, *Appl. Surf. Sci.*, 252 (2006) 2757.
27. Y. Tang and Y. Zuo, *Mater. Chem. Phys*., 88 (2004) 221.
28. M. Gholami, M. Hoseinpoor and M.H. Moayed, *Corros. Sci.*, 94 (2015) 156.
29. P.C. Pistorius and G.T. Burstein, Philos. Trans. R. Soc. London, Ser. A, 341 (1992) 531.
30. A.A. Aghuy, M. Zakeri, M.H. Moayed, M. Mazinani, *Corros. Sci.*, 94 (2015) 368.
31. R. Ke and R. Alkire, *J. Electrochem. Soc.*, 142 (1995) 4056.
32. J. Lv, T. Liang, C. Wang, T. Guo, *J. Alloys Compd.*, 658 (2016) 657.
33. M. Gholami, M. Hoseinpoor, M.H. Moayed, *Corros. Sci.*, 94 (2015) 156.
34. L. Guan, Y. Zhou, B. Zhang, J.Q. Wang, E.H. Han and W. Ke, *Int. J. Electrochem. Sci*., 11 (2016) 2326.
35. S. Asano, I. Muto, S. Yu, N. Hara, *Ecs Transactions*, 75 (2017) 9.